Ecological Informatics 46 (2018) 156–165

Contents lists available at ScienceDirect

Ecological Informatics

journal homepage: www.elsevier.com/locate/ecolinf

Spatial pattern of GPP variations in terrestrial ecosystems and its drivers: Climatic factors, CO_2 concentration and land-cover change, 1982–2015

Zhongyi Sun[a,*], Xiufeng Wang[b], Haruhiko Yamamoto[c], Hiroshi Tani[b], Guosheng Zhong[a], Shuai Yin[a], Enliang Guo[d]

[a] Hokkaido University, Graduate School of Agriculture, Kita-9 Nishi-9 Kita-Ku, Sapporo 060-8589, Japan
[b] Hokkaido University, Research Faculty of Agriculture, Kita-9 Nishi-9 Kita-Ku, Sapporo 060-8589, Japan
[c] Yamaguchi University, Faculty of Agriculture, Yoshida 1677-1, Yamaguchi 753-8515, Japan
[d] Inner Mongolia Normal University, College of Geographic Science, Hohhot 010022, China

ARTICLE INFO

Keywords:
Climate change
Atmospheric CO_2 concentration
Land-cover change
Gross primary production
Terrestrial ecosystems
C-Fix

ABSTRACT

Quantitative estimation of spatial pattern of gross primary production (GPP) trends and its drivers plays a crucial role in global change research. This study applied C-Fix model to estimate the net effect of each factor on GPP trends of 1982–2015, used an unsupervised classifier to group similar GPP trend behaviors, and analyzed the responses of GPP to changes in climatic, atmospheric and environmental drivers. According to the features of monthly GPP trends and the patterns of growing season, we presented nine categories as aids in interpreting large-scale behavior. Land-cover change (LCC), rising CO_2, temperature and water conditions changes have the positive overall effect on GPP over the entire world, contrary to radiation change effects. The global average contributions of LCC, CO_2, temperature, radiation and water on GPP trend are 4.57%, 65.73%, 13.07%, −7.24 and 11.74%, respectively. LCC and climatic factors changes have had a greater impact on GPP in terms of a specific location or regional rather than globally, and the interactions between factors are positive on GPP. The effects of climatic factors trends on GPP in different locations can be opposite, in general: regionally, GPP changes at middle and high latitudes are likely dominated by rises in radiation and temperature; at lower latitudes, GPP changes are likely to be driven by shifts in water conditions; at high altitudes, GPP changes are probably caused by changes in temperature and water conditions. These results will increase the understanding of the variations of carbon flux under future CO_2, LCC and climate conditions.

1. Introduction

Terrestrial gross primary production (GPP) is the amount of CO_2 fixed as organic compounds by vegetation through photosynthesis at the ecosystem scale (Beer et al., 2010); GPP plays a pivotal role in the global carbon balance and almost all ecosystem processes (Gilmanov et al., 2003). The patterns of the variation and distribution of GPP in terrestrial ecosystems show large spatial variability due to interactions between the biological characteristics of plants and external environmental factors (e.g., rising CO_2 concentration, land-cover change, and climatic variables) (Anav et al., 2015; Beer et al., 2010). In recent decades, approximately 1.2 PgC yr^{-1} has been sequestered by terrestrial ecosystems as the net result of the impact of the changing climate and rising CO_2 on ecosystem productivity (CO_2-climate driven flux) and deforestation, harvesting and secondary forest regrowth (land-cover change (LCC) flux) (Haverd et al., 2017). However, their contributions are highly uncertain. Therefore, it is important and necessary to accurately describe the changes of GPP in different regions and to quantitatively evaluate how environmental factors influence GPP. Furthermore, a deeper understanding of how GPP has responded to past climate change, LCC and rising CO_2 concentration will provide insight into how the carbon cycle will change under future CO_2 and climate conditions (Huang et al., 2015; Li et al., 2016; Poulter et al., 2014).

However, directly measuring GPP at the global scale is infeasible (Ma et al., 2015), and the discrepancies associated with the spatial distribution of environmental controls on GPP variation simulated by different models are considerable (Anav et al., 2015; Beer et al., 2010). In recent years, with the development of space technology, satellite-based light use efficiency (LUE) models have been widely used because they rely on simple algorithms to estimate the macroscale terrestrial GPP (Yuan et al., 2014b). In this study, the carbon fixation (C-Fix) model (Verstraeten et al., 2006) was selected to perform a series of factorial estimations to explore the drivers' net effect on GPP because in C-Fix, a CO_2 fertilization factor exists that differs from other LUE

* Corresponding author.
E-mail address: sunzy025@env.agr.hokudai.ac.jp (Z. Sun).

https://doi.org/10.1016/j.ecoinf.2018.06.006
Received 26 January 2018; Received in revised form 18 June 2018; Accepted 23 June 2018
Available online 03 July 2018
1574-9541/ © 2018 Elsevier B.V. All rights reserved.

models, and we can directly introduce the effect of the atmospheric CO_2 concentration, which is considered one of the main causes of global warming (Bazzaz, 1990; Gillett et al., 2013).

Many studies have been performed, and various models and approaches, from individual sites to global scales, have been developed and used to examine climate factors that affect GPP (Anav et al., 2015; Beer et al., 2007, 2010; de Jong et al., 2013; Liang et al., 2015; Nemani et al., 2003). Simultaneously, that CO_2 concentration effect on GPP has also been found by many scholars (Farquhar, 1997; Luo et al., 2006; Norby et al., 2005; Sun et al., 2018; Yang et al., 2016), and numerous studies (van Oijen et al., 2004; Ainsworth and Long, 2005; Yang et al., 2016) have been conducted to reveal how ecosystems respond to elevated CO_2 levels, although the magnitude and the spatial distribution of the influence remain unclear. Moreover, it is an indisputable fact that large-scale land-cover changes have taken place over the past few decades (Hansen et al., 2013; Lambin et al., 2001), and large-scale estimates of terrestrial carbon fluxes are highly dependent on the land cover (Quaife et al., 2008). However, studies that combined climate change, LCC, rising CO_2 concentration and their interactions into the effects on the pattern and trend of GPP are few.

In this study, we first used the C-Fix model to estimate the global monthly GPP over the past 34 years and tested the performance by comparing it with MTE GPP and MODIS products. Second, we analyzed the individual effect of each factor and the interactions through a series of factorial estimations around the world. Third, we zoned the categories of GPP variations according to seasonal and dimensional characteristics using an unsupervised classifier. Finally, we analyzed the GPP trend and its attribution spatially. The overarching goals of this study are to (globally during the period of 1982–2015) investigate the spatial distribution and magnitude of GPP trend; separate the contributions of climate factors, the rising CO_2 concentration, LCC and their interactions on the pattern of GPP trends spatially and quantitatively; and explain how the possible factors influence GPP in different regions.

2. Materials and methods

2.1. Materials

2.1.1. Climate data

For the global estimation of GPP, we used input datasets of sensible heat flux, latent heat flux, air temperature (T) and photosynthetically active radiation (PAR) from MERRA (Rienecker et al., 2011), which is a NASA reanalysis for the satellite era based on the main new version of the Goddard Earth Observing System Data Assimilation System Version 5 (GEOS-5) to produce an estimate of global climatic conditions at a resolution of 0.5° latitude × 0.6° longitude. More information on the MERRA dataset is available from NASA GES DISC/Modeling/ Data Holding (http://disc.gsfc.nasa.gov/daac-bin/DataHoldings.pl). The uncertainties of various meteorological factors at the global scale have been validated and evaluated by using surface metrological datasets (Li et al., 2013; Rienecker et al., 2011).

2.1.2. Vegetation indices data

The VI we used in this study, NDVI dataset, is Global Inventory Modeling and Mapping Studies (GIMMS)-3g (Tucker et al., 2005), which spanned 1982 to 2015 at a spatial resolution of 8 × 8 km^2 and a 15-day interval and was acquired from NOAA-AVHRR (Advanced Very High Resolution Radiometer). The dataset provides the only continuous and longest time series of approximately three decades that has been continually assessed and validated, and it has been widely used for long-term global vegetation condition monitoring and detecting (Liang et al., 2015; Piao et al., 2006; Wu et al., 2015). We conducted the bi-weekly data composite with pixels using the maximum value composite (MVC) method (Holben, 1986) to generate a monthly temporal scale NDVI dataset to calculate fPAR (Myneni and Williams, 1994) for running the C-Fix model.

2.1.3. Land cover data

The land cover map from 1982 to 1991 was acquired from the Global Land Cover Facility (GLCF): AVHRR Global Land Cover Classification (http://glcf.umd.edu/data/landcover/). The images from the AVHRR satellites between 1981 and 1994 were utilized and analyzed to distinguish 14 land cover classes (Hansen et al., 1998). Three spatial scales are available in this product (1, 8 km and 1°), and we selected the highest resolution of 1 km. The other is the European Space Agency (ESA) Climate Change Initiative (CCI) Land Cover (LC) dataset (https://www.esa-landcover-cci.org/), a 300 m annual global land cover time series from 1992 to 2015. These 24 annual global land cover maps were produced by state-of-the-art reprocessing of the full archives of five different satellite missions that provided daily observations of the Earth. CCI-LC provides information for 22 classes of dominant land cover types defined using the Land Cover Classification System (LCCS), which was found to be compatible with the Plant Functional Types (PFTs) used in the climate models (CCI-LC URD Phase I, 2011). Detailed information on the CCI-LC is available on the CCI-Viewer (http://maps.elie.ucl.ac.be/CCI/viewer/). The land cover data need to be crossed with the grids analyzed in this study at a 0.5° spatial resolution; all 300-m and 1-km pixels falling in the 0.5° cells were used to calculate the proportion of the dominant land cover type.

2.1.4. Atmospheric CO_2 concentration data

Two datasets of the atmospheric CO_2 concentration were used to normalize the CO_2 fertilization factor in the present study; one is the global monthly continuous spatial CO_2 concentration data from 2000 to 2015, Carbon Tracker CT2016, which is an open product of NOAA's Earth System Research Laboratory that uses data from the NOAA ESRL greenhouse gas observational network and collaborating institutions (Peters et al., 2007), released on Feb 17th, 2017. In CT2016, land biosphere, wildfire, fossil fuel emissions, atmospheric transport and other factors are data-assimilated to produce the estimates of surface fluxes and atmospheric CO_2 mole fractions (https://www.esrl.noaa.gov/gmd/ccgg/carbontracker/index.php). The other is globally averaged surface monthly mean CO_2 data from 1982 to 1999 obtained from NOAA/ ESRL (www.esrl.noaa.gov/gmd/ccgg/trends/). A global average is constructed by first fitting a smoothed curve as a function of time to each site, after which the smoothed value for each site is plotted as a function of the latitude for 48 equal time steps per year. A global average is calculated from the latitude plot at each time step (Masarie and Tans, 1995). The spatial continuous CO_2 concentration data were resampled to the 0.5° × 0.5° spatial resolution by linear method.

2.1.5. Soil property data

The Climate Prediction Center (CPC) soil moisture (SM) dataset v2 (van den Dool et al., 2003) provided by the NOAA/OAR/ESRL PSD (http://www.esrl.noaa.gov/psd/) and the Global Gridded Surfaces of Selected Soil Characteristics (IGBP-DIS) dataset (Global Soil Data Task, 2014) (http://www.daac.ornl.gov) were used in this study to calculate the water limitation on LUE by considering the stomatal regulating factor from soil moisture deficits. Since globally measuring soil moisture is impossible, we used the model-calculated CPC-SM dataset, which provides global monthly data from 1948 to 2017 consists of a file containing the averaged soil moisture water height equivalents at a spatial resolution of 0.5° × 0.5°. On the other hand, IGBP-DIS dataset is a global product generated at a resolution of 5 × 5 arc-minutes by the SoilData System (SDS), which generates soil information and maps for geographic regions at user-selected soil depths and resolutions. We used the wilting point and field capacity maps derived from this dataset and converted the data to the values at a soil depth of 1.6 m, the same as CPC-SM. The data were resampled to the 0.5° × 0.5° spatial resolution by linear method.

2.2. Model description

C-Fix is a parametric LUE model with a strong prognostic capability that is driven by plant-related, meteorological, climatic, and hydrological data to estimate carbon mass fluxes in terrestrial ecosystems (Verstraeten et al., 2006) from local (Veroustraete et al., 2002, 2004; Yuan et al., 2014a) and regional (Maselli et al., 2009; Chiesi et al., 2011;Yan et al., 2016) to global scales (Ma et al., 2015; Yuan et al., 2014b). Comparing with other LUE models, C-Fix has a module of carbon fertilization effects caused by increases in the atmospheric CO_2 concentration, which is considered to be the major reason for global warming. C-Fix can use inputs averaged over different time periods (most commonly 10-day to monthly periods) and is conceptually simple and generally applicable (Chiesi et al., 2011). For a given geographic coordinate (x, y), GPP is calculated as (Verstraeten et al., 2006):

$$GPP = PAR \times fPAR \times \varepsilon_{wl} \times T_s \times S_{CO_2} \quad (1)$$

where PAR is the incident photosynthetically active radiation, fPAR is the fractional absorbed PAR, ε_{wl} is the LUE with water stress, T_s is the temperature dependency factor, and S_{CO2} is the carbon fertilization factor due to the rising atmospheric CO_2 concentration levels. The details of calculations of the parameters can be found in the Support Materials section 1 (SM-1.1). The datasets used in this study to calculate these parameters are shown in Table 1.

2.3. Attribution method of GPP trends

Five drivers were considered for their impact on estimated GPP trends: I) rising global CO_2 concentration, II) land-cover change and changes in III) solar radiation, IV) temperature and V) water conditions. These five drivers were prescribed in the C-Fix model and the sources are introduced in Table 1. To assess the contribution of each of the five factors and possible interactions between them, we conducted a series of C-Fix factorial estimates where one driver remains fixed while the others vary during the period of 1982–2015. The estimation protocol is shown in Table 2.

The estimation with all factors varying defines the $GPP_{Control}$. In each factorial estimate (Table 2), the selected factor is held to the fixed value as the gray background in Table 2, while all other factors vary as the group of $GPP_{Control}$. In the case of "constant water, temperature and radiation", to eliminate the particularity of one year, we used the averaged values of five years from 1980 to 1984.

The individual contribution of each factor is defined as the difference, δX (X represents the individual factor), between GPP trends from each corresponding estimation and that of $GPP_{control}$ ($Trend_{control}$), in which all factors are varied (Chang et al., 2016). Since the factors influence each other, in this study, the nonlinear interaction as a residual is defined as δResidual:

$$\delta Residual = Trend_{control} - \sum_{i=1}^{n} Trend_{X_i} \quad (2)$$

where n is the number of factors and $Trend_{X_i}$ denotes the linear trend of Factorial X_i.

2.4. Study process

First, due to the different spatial resolutions of global datasets, all grid data were resampled by mean values or dominated indicators to a 0.5° × 0.5° spatial resolution. Second, all data were inputted into C-Fix to estimate the $GPP_{Control}$. We used two widely used GPP products to test the accuracy of the estimated GPP. If the accuracy of the estimates were acceptable, the factorial estimates would be calculated to obtain the estimates of $GPP_{FactorX}$. Based on the attribution method of the GPP trend, we can obtain the spatial distributions of the individual effect of each factor. We can better know the spatial and seasonal patterns of GPP variations through the monthly trend information, therefore, the GPP trend for each month of the year was calculated (e.g., the monthly GPP trends of all 34 Decembers were averaged to obtain a December trend). After spatially calculating, we got the map that shows the annual cycle of monthly GPP trends. We then calculated the monthly GPP mean values of 34 years from January to December for each pixel. Therefore, we can obtain information on the vegetation average growing situation in one year to represent the annual cycle of growing season. The two annual cycles revealed the month of one year when GPP increases or decreases at a given location were caused by changes in the GPP amplitude or the growing season length (Hicke et al., 2002); and we draw the description figure following Hicke et al. (2002) as Fig. 2. We used this characteristic as the index of vegetation growth changes in the cluster classification to obtain the spatial distribution of the GPP change types. Finally, according to the spatial distribution of each factor monthly trends, net effects and GPP change types, we will more clearly understand the spatial patterns and the drivers of GPP variations. Fig. 1 shows the logical process of this study.

3. The results

3.1. Accuracy assessment of estimated GPP

In this study, we estimated a relative long-term series global GPP at a spatial resolution of 0.5°, which is larger than the footprint size of ground-based observations. Hence, we relied on the model and other remotely sensed data for a comparison on the global scale. As a benchmark, we compared the estimates against the MTE model GPP from 1982 to 2011 (Jung et al., 2011) because it is based on direct eddy-covariance flux tower measurements of GPP and is thus considered close to the truth where the flux tower density is high (Beer et al., 2010; Frankenberg et al., 2011). MODIS GPP products from 2000 to 2014 were also used because MODIS products have been widely known and used (Frankenberg et al., 2011; Turner et al., 2006b; Zhao and Running, 2010). As well as the results from process-based models of 1982–2010 from the Inter-Sectoral Impact Model Intercomparison

Table 1
Overview of the datasets used in this study.

Data used to estimate GPP	Datasets /products	Period	Resolution	Data source / acquisition
NDVI	GIMMS-3g	1982–2015	8 km × 8 km	NOAA AVHRR
Land-cover classification	UMD Land-cover Classification	1981–1994	1 km × 1 km	GLCF
	CCI-LC	1992–2015	300 m × 300 m	ESA
Atmospheric CO_2 concentration	CO_2 records	1982–1999	global	NOAA ESRL
	CT2016	2000–2015	2° latitude × 3° longitude	
Photosynthetically active radiation	MERRA	1980–2015	0.5° latitude × 0.6° longitude	NASA GES DISC
Air temperature				
Sensible heat flux				
Latent heat flux				
Soil moisture	CPC-SM v2	1980–2015	0.5° × 0.5°	NOAA ESRL PSD
Wilting point & field capacity	IGBP-DIS	1950–1996	0.5° × 0.5°	NASA ORNL DAAC

Table 2
Illustration of the estimation protocol and the five factors used as input data for factorial estimates.

Factorial estimates	Water forcing	Temperature forcing	Radiation forcing	CO_2 level increasing	Land-cover change
$GPP_{Control}$	1982-2015	1982-2015	1982-2015	1982-2015	1982-2015
GPP_{Water}	**1980-1984**	1982-2015	1982-2015	1982-2015	1982-2015
$GPP_{Temperature}$	1982-2015	**1980-1984**	1982-2015	1982-2015	1982-2015
$GPP_{Radiation}$	1982-2015	1982-2015	**1980-1984**	1982-2015	1982-2015
GPP_{CO2}	1982-2015	1982-2015	1982-2015	**1982**	1982-2015
GPP_{LCC}	1982-2015	1982-2015	1982-2015	1982-2015	**1982**

Project II (ISIMIP2a) (Chang et al., 2017; Reyer et al., 2017) were selected to test the accuracy of estimated GPP. For the annual GPP, we found a strong linear spatial correlation between the estimated GPP with process-based models, MTE and remotely sensed GPP values, most notably with MTE_GL GPP (averaged $r = 0.9269$, averaged slope = 1.0977), followed by MTE_MR GPP (averaged $r = 0.9266$, averaged slope = 1.1008) and MODIS GPP (averaged $r = 0.9205$, averaged slope = 1.3089) (SM 2.1). The performs of the comparing with the results from different process-based models were different (SM 2.3), but all show a strong correlation. Compared with the results of multiple models, the spatial correlation coefficient could reach 0.8377 with the slope of 1.0159. We find that the estimated GPPs are highly consistent with MTE GPP and MODIS products; thus, the estimated GPP in the present study can be used in subsequent analyses.

3.2. GPP trends

3.2.1. Contributions of different factors to GPP trends

For the global terrestrial ecosystems, the overall effect of all the five factors considered is positive (Table 3). The key result is that the increases in the atmospheric CO_2 concentration make the largest contribution to the globally averaged GPP trend. The changes in water conditions and temperature caused comparable but lower GPP positive trends. The changes in solar radiation caused the whole effect of decreasing GPP. Although the change in GPP attributed to land-cover change is positive around the world, the regional maximum negative

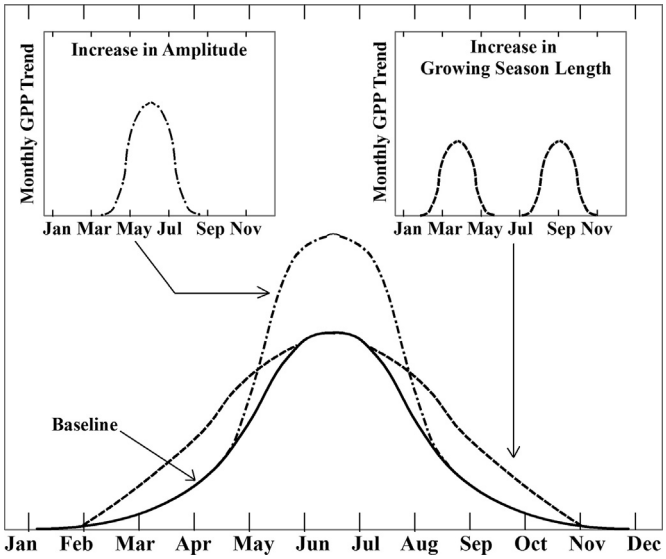
Increase in Amplitude
Increase in Growing Season Length
Monthly GPP Trend
Jan Mar May Jul Sep Nov
Baseline
Jan Feb Mar Apr May Jun Jul Aug Sep Oct Nov Dec

Fig. 2. Schematic showing monthly trends in GPP in response to an increase in the amplitude if the GPP annual cycle (dashed-dotted curve) and an increase in the length of the growing season (dashed curve) occurred from a baseline GPP annual cycle (solid curve).

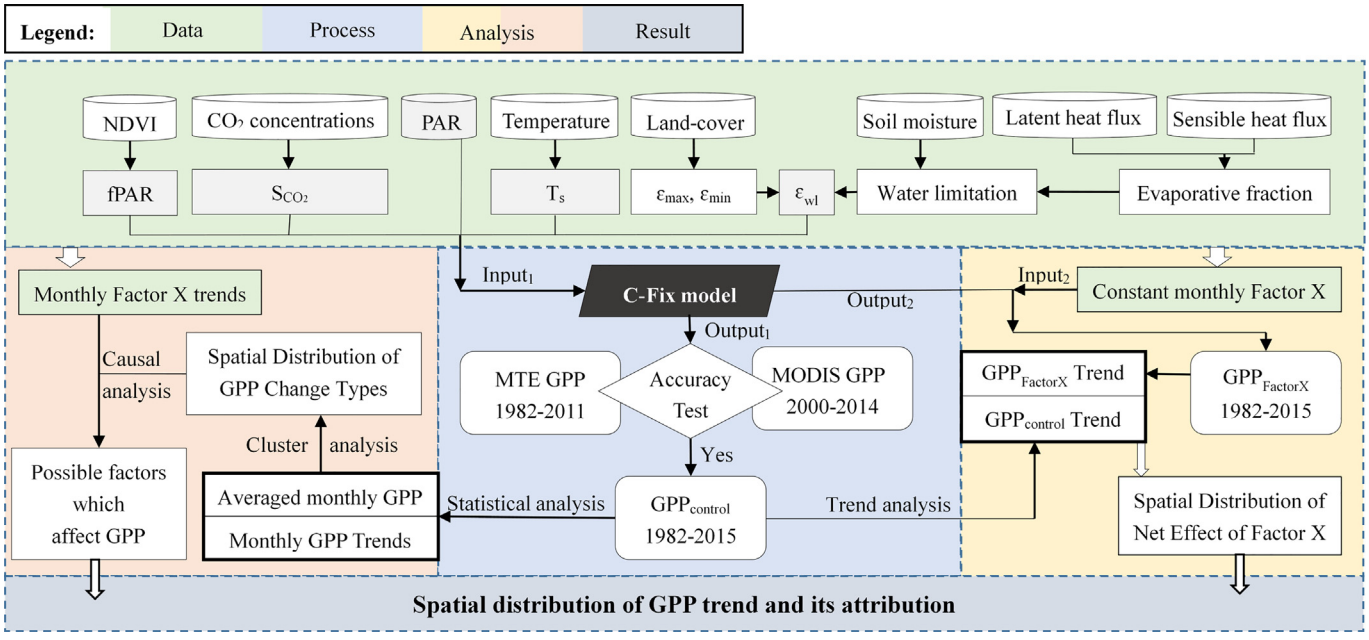

Fig. 1. Study flowchart.

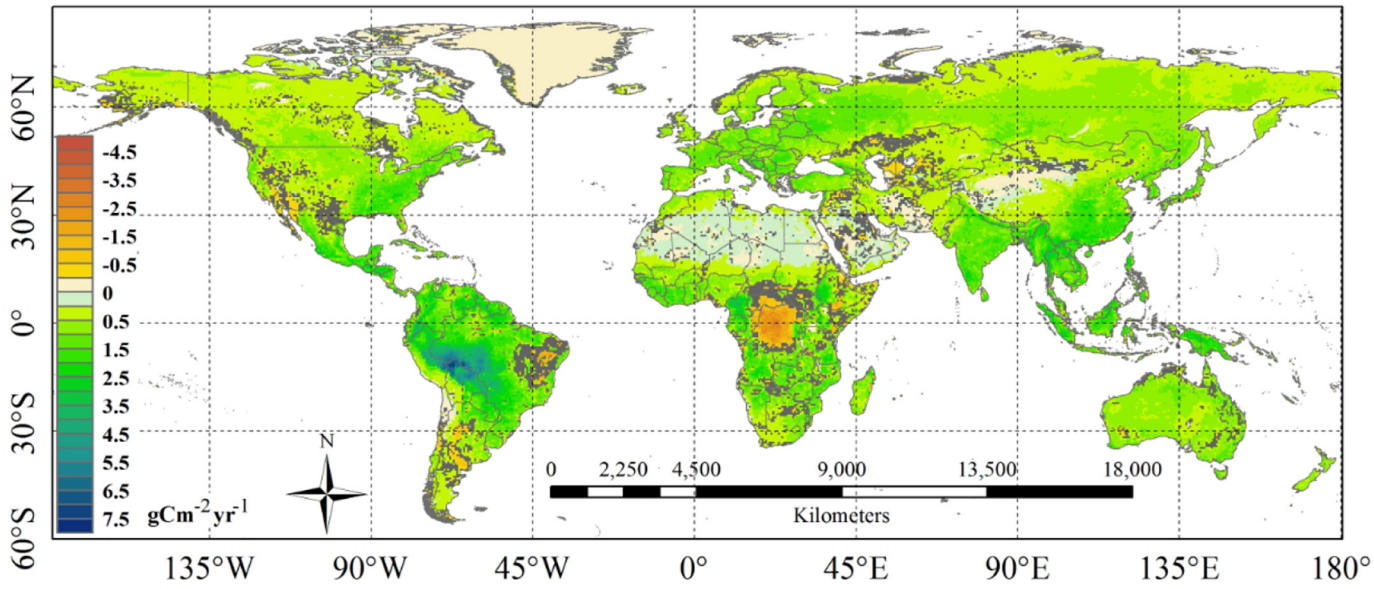

Fig. 3. The spatial distribution of linear trends in GPP during the period 1982–2015. The pixels that are not satisfied at p_value < 0.1 are drawn in gray.

effect also occurred due to land-cover changes. That the sum of the effects of each factor on GPP trends is 0.0795 $gCm^{-2}yr^{-1}$ smaller than the overall GPP trend attributed to all factors indicates that the interactions between each factor are positive.

3.2.2. Spatial distribution of the GPP trend and its attribution

The spatial distribution of annual GPP trend in the period of 1982–2015 is shown in Fig. 3. The contribution of different factors in different areas vary considerably (Fig. 4). The figure shows that the largest increases in GPP are found in the southern parts of the Amazon rainforest with increases of 5 $gCm^{-2}yr^{-1}$, where the changes in temperature and water conditions play the major roles in causing the increasing GPP trends (Fig. 4). Positive GPP trends > 3 $gCm^{-2}yr^{-1}$ were found in the InterTropical Convergence Zone (ITCZ) except for Congo rainforest, which has the largest decreases in GPP with values that exceed -2 $gCm^{-2}yr^{-1}$, where the changes in water conditions and the enhanced interactions play the most important roles in explaining those GPP trends. Followed by humid temperature regions in eastern North America, western and central Europe and eastern China, with an increment of approximately 2.5 $gCm^{-2}yr^{-1}$ is found, and solar radiation and temperature have positive effects on GPP trends. Not all regions show the positive GPP trends, we also found negative GPP trends in the Borbolima Plateau, Diamantine Plateau, Pampas grassland, Cordillera Mountains, Australian desert and the areas east of Caspian Sea. And relatively concentrated are the trends of the Congo Basin which were attributed to the effect of the changes in temperature and water conditions.

The changes in the atmospheric CO_2 concentration make almost no negative contribution to the pattern of the GPP trend globally. Significant positive GPP trend effects of land-cover changes were found in regions such as high latitudes, mid-latitudes inland areas, high altitude areas and some barren vegetation areas. In contrast, in many areas, especially the dry forest of South America and eastern Africa and the Eurasian rainforest, the land-cover change shows a decreasing GPP effect. Regarding contributions of climatic factors (temperature, water, and radiation), regionally, climate change can have either a positive or a negative effect on GPP trends. In addition, the interactions among different factors also have regional characteristics.

3.3. GPP trend category zoning

To further investigate the seasonal dynamics and varying patterns of

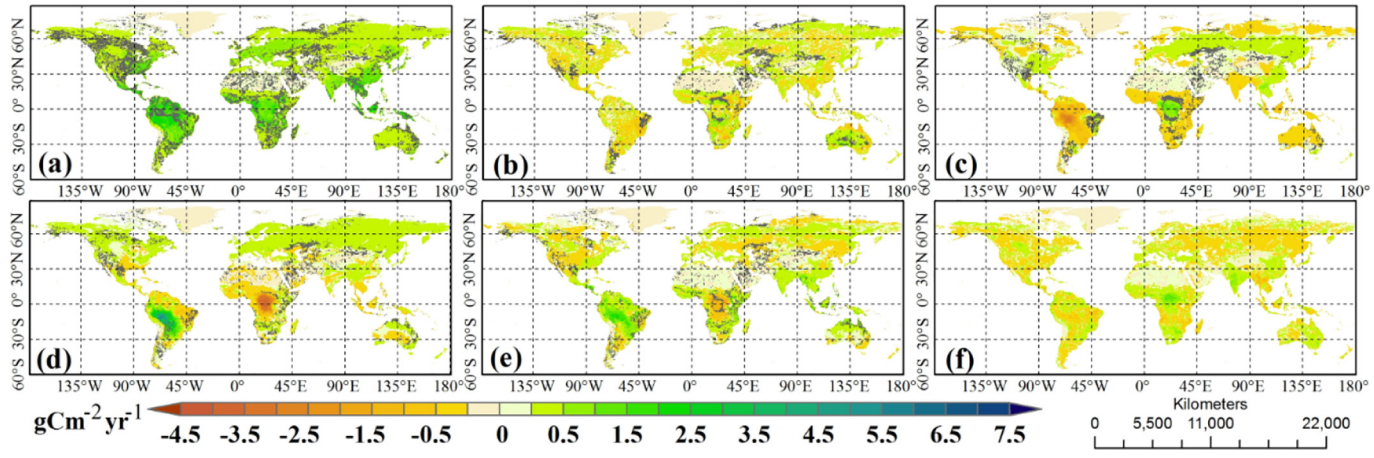

Fig. 4. Spatial distribution of the trends in GPP due to (a) increases in atmospheric CO_2 concentration, (b) land-cover change, (c) solar radiation changes, (d) temperature changes, (e) changes in water conditions, and (f) their nonlinear interactions or non-attributed. The pixels ((a) to (e)) that are not satisfied at p_value < 0.1 are drawn in gray.

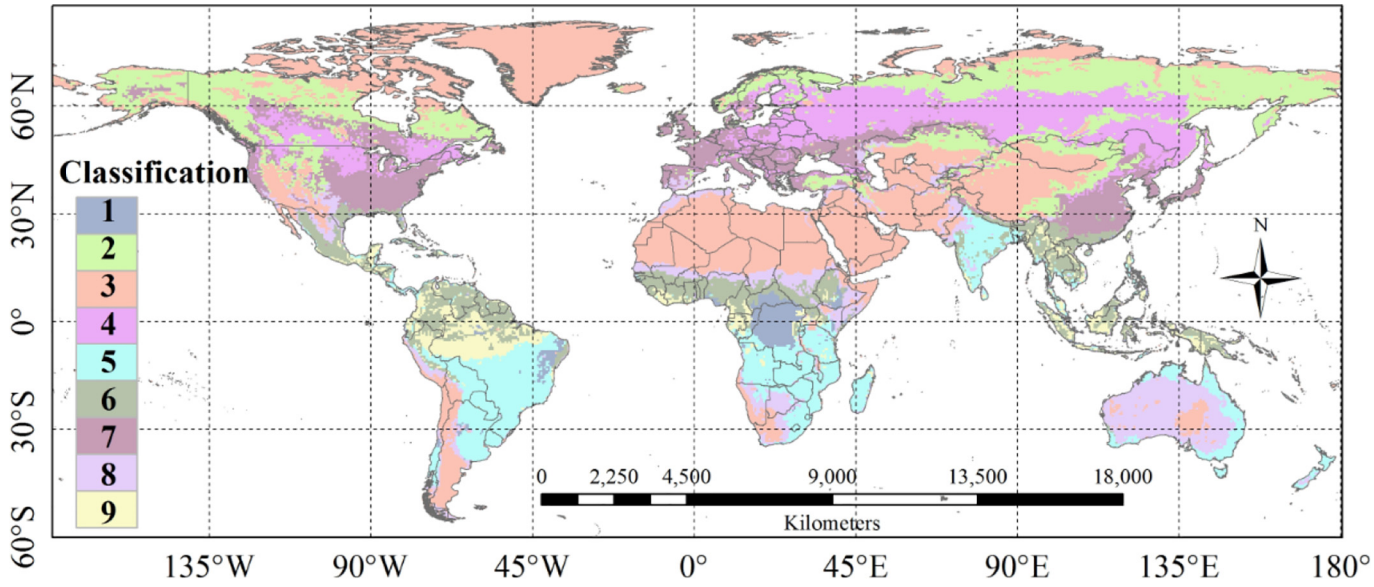

Fig. 5. The spatial distribution of classes on variations in GPP during the period 1982–2015.

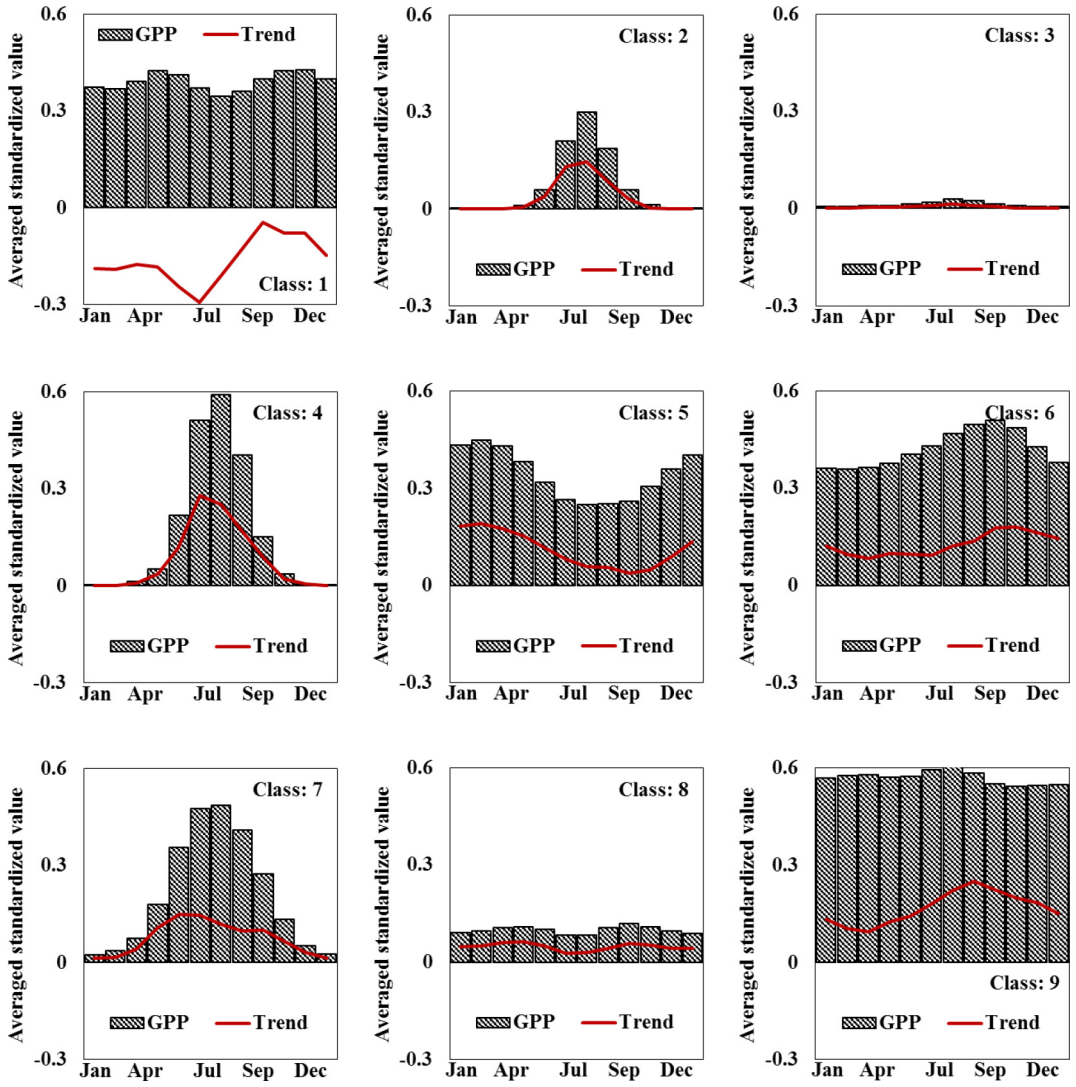

Fig. 6. Characteristics of the annual cycle of the growing season distribution and GPP trends associated with each class.

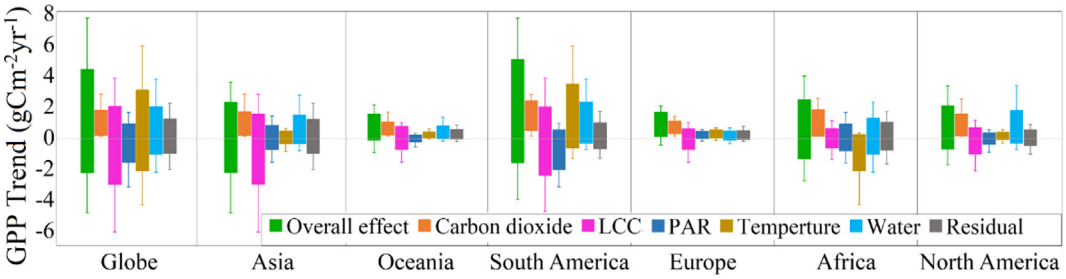

Fig. 7. The range of contributions of GPP to different factors globally and on each continent (The bottom of the box is the lower quartile, and the top is the upper quartile. The whiskers extend to the maximum and minimum values).

GPP during the period of 1982–2015, we classified the monthly GPP and monthly GPP trends to group locations with similar behaviors. This isolated regions that had lengthening growing seasons, for example, or had increased GPP in the rapid growth stage (RGS). We used the average monthly GPP in the classification as an index of the vegetation growth stage. The monthly GPP and GPP trends were first normalized to allow these variables to be used together in the classification (Hicke et al., 2002).

Nine general categories (Fig. 5) resulted from using a k-means (Hartigan, 1975) classifier according to the statistical characteristics information of GPP variations. Here, we focus our results on the large-scale patterns that occurred. Because specifying fewer groups obscured some information in the analysis, and although the classification assigns each pixel to a group and we present the class mean information (Fig. 6), we have to admit that the circumstance that a pixel may not behave in a manner close to the class mean exists. This categorization is necessarily approximate; we used the groups as an aid to explain the large-scale behavior of GPP variations: Class 1: Mainly in the African rainforest, GPP trends are negative, especially in July between two RGSs; the first RGS ends early and the second RGS has a delayed start; Class 2: Mainly in high latitudes and high altitudes, GPP trends are positive, and the main reason for the increasing GPP is the changes in the amplitude. Class 3: Mainly in polar and barren areas, there are low or almost no GPP in these areas, and the increases or decreases are almost equal to 0; Class 4: Mainly in cool temperate zones, GPP trends are positive, and the RGS has an early lengthening trend. However, the changes in the amplitude play a more important role. In Class 5, mainly in equatorial, winter dry climate zones, the GPP trends are positive throughout the growing season; and the increasing trend in the early period is less than that in the middle and later periods. The RGS has a trend of delayed ends; Class 6: Mainly in equatorial, fully humid climate zones, the GPP trends were positive throughout the growing season, and the end of the RGS has a slightly delayed trend. In Class 7: Mainly in warm temperate zones, the curve of the GPP trends are similar to a bimodal curve, and the trend of lengthening in growing season is obvious; Class 8: Mainly distributed in desert areas, the vegetation has two RGSs, and the increment in the first RGS is larger than that in the second RGS; Class 9: Mainly distributed in the fully humid zones of Amazon rainforest, the GPP is stable at a high level throughout the year, and the RGS extends backwards.

4. Discussions

4.1. Increases in atmospheric CO_2 concentration

In this study, the contribution of the rising CO_2 concentration on the globally averaged GPP trend is the largest proportion. However, we cannot conclude that the effect of the increasing CO_2 concentration on GPP variations is more important than the changes in other factors. The main reason is that the increases in the CO_2 concentration occurred in a globally synchronous manner, while the global averaged effects of the other factors are neutralized because the attributions can be positive or negative in different locations (Fig. 7). An elevated atmospheric CO_2 concentration enhances vegetation photosynthesis and has indirect effects on increasing water use efficiency (Donohue et al., 2013; Fensholt et al., 2012), and in this study, we can see that the regions with a relatively larger increasing GPP trend also had better water condition trends (e.g., Asian rainforest, Amazon rainforest, eastern Africa, and large areas in the middle-high latitudes in the Northern Hemisphere). In our estimation, the rising CO_2 concentration causes an average of a 2.63% increase around the globe over 34 years which falls within the range of a sensitivity analysis on GPP affected by increasing CO_2 (Wang et al., 2014). Models that do not consider CO_2 fertilization modules might be a source of uncertainty (Anav et al., 2015) in estimating GPP, and elevated atmospheric CO_2 concentration is one of the main reasons for global climate change. Therefore, we used the C-Fix model, which has a carbon fertilization module instead of other LUE models such as the CASA (Potter et al., 1993), CFlux (Turner et al., 2006a) VPM (Xiao et al., 2004), VPRM (Mahadevan et al., 2008), EC-LUC (Yuan et al., 2007) and MODIS-GPP algorithms (Running et al., 2000). We used the MTE GPP and MODIS product to compare our estimated GPP and found that we estimated a higher GPP than the MTE GPP and MODIS product. The relationship with MODIS GPP is consistent with previous studies (Anav et al., 2015; Heinsch et al., 2006), which reported that the products are smaller than the GPP observed at many flux tower sites. The growth rate of the slopes of our estimated GPP on the MODIS product shows a significant correlation with the trend of rising CO_2 concentrations with a correlation coefficient of 0.9290. This finding can better illustrate that without considering carbon, fertilization is the main reason for the lower values in MODIS product. Regarding the comparison with MTE GPP, our estimates are larger than MTE GPP,

Table 3
Trends in GPP globally during the period 1982–2015 and the effects of the factors on the trend.

Factors	Average effect*	Max effect*	Min effect*	Standard deviation*	Globally averaged contribution%	Positive effect fraction%
Overall effect	0.6560	7.6213	−4.9341	0.7811	100.00	75.76
Temperature	0.0857	5.8234	−4.4056	0.5412	13.07	73.16
Water	0.0770	3.6817	−2.3074	0.2944	11.74	42.68
Radiation	−0.0475	1.5470	−3.2759	0.3480	−7.24	35.74
CO_2 concentration	0.4312	2.7181	−0.0027	0.5088	65.73	57.74
LCC	0.0300	3.7428	−6.1646	0.2244	4.57	63.08
Residual	0.0795	2.1355	−2.5261	0.2115	12.13	46.23

* All values are at the level of p_value < 0.1, and the unit is $gCm^{-2}yr^{-1}$.

with an average slope of 1.1985 from 1982 to 2011, with the trend of following the rising CO_2 concentration. This result is almost the same as the finding by Piao et al. (2013), who used 10 process-based terrestrial biosphere models used for the IPCC Fifth Assessment Report compared to MTE GPP, and the models were found to produce a higher GPP than MTE with a trend of 1.1271 from 1982 to 2008. Therefore, our estimates can successfully reflect the effect of elevated CO_2 concentration on GPP during the period of 1982–2015.

4.2. Effects of LCC

For the globe, the greatest negative impact on the GPP trend is from LCC, which has a direct effect on PFTs (Chen et al., 2006). These negative effect areas are concentrated in South America (especially Brazil, Argentina, Bolivia and Paraguay)(Jepson, 2005), Eurasian rainforests (especially Indonesia), and tropical dry forests in Africa (especially Ethiopia), all of which had the highest rate of forest loss (Lepers et al., 2005; Hansen et al., 2013; Gibbs et al., 2010). In addition, the rates of forest loss were relative lower in the temperate climate zones of North America and Europe, where the LCC also had a relatively lower negative effect on GPP. In Europe and Oceania, the latitudinal span is not as great as on other continents; therefore, the range of the effects of radiation, water and temperature are relatively consistent, and the most significant spatial difference effect is from LCC (Fig. 7).

4.3. Effects of climatic factors on GPP

The changes in the temperature and water over the past 34 years are estimated to cause increases in GPP around the world as a whole, which is contrary to the results caused by changes in radiation. However, the effect of these factor trends can be positive or negative in different regions. To further investigate the possible climate drivers that cause the seasonal dynamics and varying patterns of GPP during the period of 1982–2015, we analyzed the monthly trends for each factor (SM2.4) and summarized the distribution of the regions where GPP has varied due to different possible drivers.

The productivity of vegetation in tropical dry zone is weak; climate change induces a slight trend in GPP in those regions. The GPP trends in tropical wet zones (i.e. Indonesian- Malaysian rainforest, Latin America) are positive because their dominant factor, water conditions, have become increasingly suitable for vegetation growth, which is also suitable for the high altitudes in Africa. In cool temperate moist zones, the positive trend is the result from the early growing season lengthening caused by radiation shifts and plant growth enhancement caused by temperature and radiation changes. With respect to cool temperate dry zones, the positive effects of the temperature and radiation during the rapid growth stage are the main drivers causing increases in the amplitude of vegetation growth. For most warm temperate dry zones, the changes of the GPP are dominated by radiation; hydrothermal conditions in the regions are almost unchanged during the growing season (from May to September). Conversely, radiation and water conditions together led to an increasing GPP trend in warm temperate moist zones, where water condition changes enhance the plant growth magnitudes and radiation lengthens the growing season. Additionally, in tropical moist zones, the evapotranspiration is reduced by the decreasing temperature; simultaneously, the water conditions become more suitable for plant growth. Therefore, the GPP trends are positive. Moreover, in South America, the growing season length has been extended by increased radiation in the later period of the rapid growth stage. In boreal moist zones, radiation and hydrothermal conditions in the growing season jointly promote vegetation growth. Regarding polar moist zones, in September, the rapid growth stage has an early end due to the declining radiation, but the water conditions and temperature elevating the GPP magnitude during the growing season result in a positive effect. For Congo Basin and Brazilian Highlands where following by increasing temperatures and decreasing water the monthly GPP decreased mostly. The Congo rainforest has some continental climate characteristics, where water is the dominant factor inducing the trend in GPP. Water conditions become more unsuitable; although radiation became more abundant, it is accompanied by increasing temperatures and evapotranspiration, ultimately inducing a negative trend in GPP. Additionally, in South Central Australia, three factors contribute to the conditions: water conditions dominate the GPP changes, including the magnitudes and growing season length; radiation increased during the later growth period; and temperatures became more suitable during the growing season.

Combined with terrain and location, we can generally and summarily conclude that radiation and temperature are relatively sufficient for vegetation in lower latitudes since solar irradiation occurs twice a year. Therefore, water conditions have become the dominant climatic factor affecting GPP trends. In addition, adequate water conditions are associated with decreasing radiation due to cloud cover and reducing temperature due to evaporation. Hence, the trends of GPP in lower latitudes are also affected by radiation and temperature synergistically, while in the middle and high latitudes, the main climatic factors affecting GPP trends are temperature and radiation, which have improved the demand for suitable conditions during the growing season and explains much of the increasing GPP trends in temperature and radiation variability in the northern regions of North America and Eurasia. Additionally, in high altitude regions, since the hydrothermal conditions are further from the ideal situation, temperature and water conditions are the main climatic factors in GPP trends in these regions.

5. Conclusions

In this study, we estimated the global monthly GPP at a $0.5^\circ \times 0.5^\circ$ spatial resolution during the period of 1982–2015, analyzed the effects of drivers on GPP trend and zoned the categories of GPP variation.

The five factors considered in this study resulted in an overall positive effect on the GPP trend but with different spatial patterns, magnitudes, and mechanisms. Globally, increases in GPP occurred in over 75% of the areas; the interactions between factors were positive, and the increases in atmospheric CO_2 concentration had the greatest contribution on global increasing GPP. However, regionally, the LCC and climatic factors appear play more important roles in GPP changes.

Larger areas in the lower latitudes showed increases in the amplitude of the GPP annual cycle which dominated by shifts in water conditions; in contrast, in the middle latitudes GPP expressed not only the amplitude changes but also a lengthened rapid growth stage during the early period which were likely to be driven by increases in temperature and radiation; in large areas of the Southern Hemisphere, GPP increased in both the early and later period of the growing season, resulting in a lengthening growing season. However, at high altitudes, the changes in GPP were probably caused by the changes in the temperature and water conditions.

The CO_2 fertilization effect was explicitly expressed in this study by comparisons with MTE and MODIS GPP. By contrast, the effect of nutrition cannot be quantified from our study since any resulting changes were implicit in the satellite-observed NDVI and were not explicitly modeled. Many studies show that nutrient availability strongly constrains vegetation growth through water availability, the CO_2 assimilation rate and other factors (Reich et al., 2014; Wieder et al., 2015). The potential effects of nutrient limitation should be considered in estimates of the terrestrial GPP in future studies.

In summary, we found a wide range of GPP trends, both spatially and seasonally. It appears that CO_2, LCC and climatic factors together played a role in global terrestrial GPP changes.

Acknowledgements

This study was supported by Scientific Research (B), 15H05256 (PI: Prof. Haruhiko Yamamoto, Yamaguchi University, Japan). We

gratefully acknowledge ISIMIP2, IGBP, GLCF, ESA, NASA and NOAA for providing data that were used in this study. We thank ISIMIP/ESGF (https://esg.pik-potsdam.de/search/isimip/), NOAA/OAR/ESRL PSD (http://www.esrl.noaa.gov/psd/), (http://carbontracker.noaa.gov) and (www.esrl.noaa.gov/gmd/ccgg/trends/), ORNL DAAC (http://webmap.ornl.gov/wcsdown/), GMAO (https://gmao.gsfc.nasa.gov/) and CCIViewer (http://maps.elie.ucl.ac.be/CCI/viewer/) for allowing us to download various climate (air temperature, sensible heat flux, latent heat flux, solar radiation), GPP products (CARAIB, DLEM, JULES-B1, LPJml, ORCHIDEE, VEGAS, VISIT), geospatial data (MODIS NDVI, GPP), soil data (soil moisture), atmospheric CO_2 records (CarbonTracker CT2016 and long-term CO_2 record) and land-cover datasets. We also thank Mr. Jung and Projects of BGI and GEOCARBON for making and providing access to the MTE GPP data.

References

Ainsworth, E.A., Long, S.P., 2005. What have we learned from 15 years of free-air CO_2 enrichment (FACE)? A meta-analytic review of the responses of photosynthesis, canopy properties and plant production to rising CO_2. New Phytol. 165, 351–372.

Anav, A., Friedlingstein, P., ... Zhao, M.S., 2015. Spatiotemporal patterns of terrestrial gross primary production: a review. Rev. Geophys. 53, 785–818.

Bazzaz, F.A., 1990. The response of natural ecosystems to the rising global CO2 levels. Annu. Rev. Ecol. Syst. 21, 167–196.

Beer, C., Reichstein, M., ... Papale, D., 2007. Mean annual GPP of Europe derived from its water balance. Geophys. Res. Lett. 34.

Beer, C., Reichstein, M., ... Bonan, G.B., 2010. Terrestrial gross carbon dioxide uptake: global distribution and covariation with climate. Science 329, 834–838.

CCI-LC URD Phase I, 2011. Land Cover Climate Change Initiative - User Requirements Document. Issue 2.2.Date 23.02.. .

Chang, J., Ciais, P., ... Soussana, J.F., 2016. Effect of climate change, CO2 trends, nitrogen addition, and land–cover and management intensity changes on the carbon balance of European grasslands. Glob. Chang. Biol. 22, 338–350.

Chang, Jinfeng, et al., 2017. Benchmarking carbon fluxes of the ISIMIP2a biome models. Environ. Res. Lett. 12 (4), 045002.

Chen, H., Tian, H., ... Zhang, C., 2006. Effect of land-cover change on terrestrial carbon dynamics in the southern United States. J. Environ. Qual. 35, 1533–1547.

Chiesi, M., Fibbi, L., ... Vaccari, F.P., 2011. Integration of ground and satellite data to model Mediterranean forest processes. Int. J. Appl. Earth Obs. Geoinf. 13, 504–515.

Donohue, R.J., Roderick, M.L., ... Farquhar, G.D., 2013. Impact of CO2 fertilization on maximum foliage cover across the globe's warm, arid environments. Geophys. Res. Lett. 40, 3031–3035.

Farquhar, G.D., 1997. Carbon dioxide and vegetation. Science 278, 1411.

Fensholt, R., Langanke, T., ... Eastman, R., 2012. Greenness in semi-arid areas across the globe 1981–2007—an Earth Observing Satellite based analysis of trends and drivers. Remote Sens. Environ. 121, 144–158.

Frankenberg, C., Fisher, J.B., ... Kuze, A., 2011. New global observations of the terrestrial carbon cycle from GOSAT: patterns of plant fluorescence with gross primary productivity. Geophys. Res. Lett. 38.

Gibbs, H.K., Ruesch, A.S., ... Foley, J.A., 2010. Tropical forests were the primary sources of new agricultural land in the 1980s and 1990s. Proc. Natl. Acad. Sci. 107, 16732–16737.

Gillett, N.P., Arora, V.K., ... Allen, M.R., 2013. Constraining the ratio of global warming to cumulative CO2 emissions using CMIP5 simulations. J. Clim. 26, 6844–6858.

Gilmanov, T.G., Verma, S.B., ... Suyker, A.E., 2003. Gross primary production and light response parameters of four Southern Plains ecosystems estimated using long-term CO2-flux tower measurements. Glob. Biogeochem. Cycles 17 n/a-n/a.

Global Soil Data Task, 2014. Global Soil Data Products CD-ROM Contents (IGBP-DIS). ORNL DAAC, Oak Ridge, Tennessee, USA. http://dx.doi.org/10.3334/ORNLDAAC/565.

Hansen, M., DeFries, R., Townshend, J.R.G., Sohlberg, R., 1998. UMD Global Land Cover Classification, 1 Kilometer, 1.0. Department of Geography, University of Maryland, College Park, Maryland, pp. 1981–1994.

Hansen, M.C., Potapov, P.V., ... Loveland, T., 2013. High-resolution global maps of 21st-century forest cover change. Science 342, 850–853.

Hartigan, J., 1975. The K-means algorithm. Clustering algorithms 4.

Haverd, V., Smith, B., ... Canadell, J., 2017. A novel assessment of the role of land-use and land-cover change in the global carbon cycle, using a new dynamic global vegetation model version of the CABLE land surface model. In: EGU General Assembly Conference Abstracts, pp. 13881.

Heinsch, F.A., Zhao, M.S., ... Flanagan, L.B., 2006. Evaluation of remote sensing based terrestrial productivity from MODIS using regional tower eddy flux network observations. IEEE Trans. Geosci. Remote Sens. 44, 1908–1925.

Hicke, J.A., Asner, G.P., Randerson, J.T., ... Field, C., 2002. Trends in north American net primary productivity derived from satellite observations, 1982–1998. Glob. Biogeochem. Cycles 16.

Holben, B.N., 1986. Characteristics of maximum-value composite images from temporal AVHRR data. Int. J. Remote Sens. 7, 1417–1434.

Huang, M., Piao, S., ... Wang, Y., 2015. Change in terrestrial ecosystem water-use efficiency over the last three decades. Glob. Chang. Biol. 21, 2366–2378.

Jepson, W., 2005. A disappearing biome? Reconsidering land-cover change in the Brazilian savanna. Geogr. J. 171, 99–111.

de Jong, R., Schaepman, M.E., ... Verburg, P.H., 2013. Spatial relationship between climatologies and changes in global vegetation activity. Glob. Chang. Biol. 19, 1953–1964.

Jung, M., Reichstein, M., ... Williams, C., 2011. Global patterns of land-atmosphere fluxes of carbon dioxide, latent heat, and sensible heat derived from eddy covariance, satellite, and meteorological observations. J. Geophys. Res-Biogeo 116.

Lambin, E.F., Turner, B.L., ... Folke, C., 2001. The causes of land-use and land-cover change: moving beyond the myths. Glob. Environ. Chang. 11, 261–269.

Lepers, E., Lambin, E.F., ... Scholes, R.J., 2005. A synthesis of information on rapid land-cover change for the period 1981–2000. AIBS Bull. 55, 115–124.

Li, X., Liang, S., Yu, G., ... Ma, M., 2013. Estimation of gross primary production over the terrestrial ecosystems in China. Ecol. Model. 261, 80–92.

Li, X., Zhu, Z., ... Piao, S., 2016. Estimation of gross primary production in China (1982–2010) with multiple ecosystem models. Ecol. Model. 324, 33–44.

Liang, W., Yang, Y., ... Bai, D., 2015. Analysis of spatial and temporal patterns of net primary production and their climate controls in China from 1982 to 2010. Agric. For. Meteorol. 204, 22–36.

Luo, Y., Hui, D., Zhang, D., 2006. Elevated CO2 stimulates net accumulations of carbon and nitrogen in land ecosystems: a META–analysis. Ecology 87, 53–63.

Ma, J., Yan, X., ... Chou, J., 2015. Gross primary production of global forest ecosystems has been overestimated. Sci. Rep. 5, 10820.

Mahadevan, P., Wofsy, S.C., ... Gottlieb, E.W., 2008. A satellite-based biosphere parameterization for net ecosystem CO2 exchange: vegetation photosynthesis and respiration model (VPRM). Glob. Biogeochem. Cycles 22.

Masarie, K.A., Tans, P.P., 1995. Extension and integration of atmospheric carbon-dioxide data into a globally consistent measurement record. J. Geophys. Res.-Atmos. 100, 11593–11610.

Maselli, F., Papale, D., ... Corona, P., 2009. Combining remote sensing and ancillary data to monitor the gross productivity of water-limited forest ecosystems. Remote Sens. Environ. 113, 657–667.

Myneni, R., Williams, D., 1994. On the relationship between FAPAR and NDVI. Remote Sens. Environ. 49, 200–211.

Nemani, R.R., Keeling, C.D., ... Running, S.W., 2003. Climate-driven increases in global terrestrial net primary production from 1982 to 1999. Science 300, 1560–1563.

Norby, R.J., Delucia, E.H., ... Ceulemans, R., 2005. Forest response to elevated CO2 is conserved across a broad range of productivity. Proc. Natl. Acad. Sci. U. S. A. 102, 18052–18056.

Peters, W., Jacobson, A.R., ... Tans, P.P., 2007. An atmospheric perspective on North American carbon dioxide exchange: CarbonTracker. Proc. Natl. Acad. Sci. U. S. A. 104, 18925–18930. http://dx.doi.org/10.1073/pnas.0708986104.

Piao, S., Fang, J., Zhou, L., Ciais, P., Zhu, B., 2006. Variations in satellite-derived phenology in China's temperate vegetation. Glob. Chang. Biol. 12, 672–685.

Piao, S., Sitch, S., ... Huntingford, C., 2013. Evaluation of terrestrial carbon cycle models for their response to climate variability and to CO2 trends. Glob. Chang. Biol. 19 (7), 2117–2132.

Potter, C.S., Randerson, J.T., ... Klooster, S.A., 1993. Terrestrial ecosystem production: a process model based on global satellite and surface data. Glob. Biogeochem. Cycles 7, 811–841.

Poulter, B., Frank, D., ... Liu, Y.Y., 2014. Contribution of semi-arid ecosystems to interannual variability of the global carbon cycle. Nature 509, 600.

Quaife, T., Quegan, S., ... Woodward, F., 2008. Impact of land-cover uncertainties on estimates of biospheric carbon fluxes. Glob. Biogeochem. Cycles 22.

Reich, P.B., Hobbie, S.E., Lee, T.D., 2014. Plant growth enhancement by elevated CO2 eliminated by joint water and nitrogen limitation. Nat. Geosci. 7, 920.

Reyer, Christopher, Asrar, Gassem, Betts, Richard, et al., 2017. ISIMIP2a simulation data from biomes sector. GFZ Data Serv. http://dx.doi.org/10.5880/PIK.2017.002.

Rienecker, M.M., Suarez, M.J., Gelaro, R., et al., 2011. MERRA: NASA's modern-era retrospective analysis for research and applications. J. Clim. 24, 3624–3648.

Running, S.W., Thornton, P.E., ... Glassy, J.M., 2000. Global Terrestrial Gross and Net Primary Productivity from the Earth Observing System. pp. 44–57.

Sun, Z., Wang, X., ... Yin, S., 2018. An attempt to introduce atmospheric CO2 concentration data to estimate the gross primary production by the terrestrial biosphere and analyze its effects. Ecol. Indic. 84, 218–234.

Tucker, C.J., Pinzon, J.E., Brown, M.E., et al., 2005. An extended AVHRR 8-km NDVI dataset compatible with MODIS and SPOT vegetation NDVI data[J]. Int. J. Remote Sens. 26 (20), 4485–4498.

Turner, D., Ritts, W., ... Law, B., Thornton, P., 2006a. A diagnostic carbon flux model to monitor the effects of disturbance and interannual variation in climate on regional NEP. Tellus B 58, 476–490.

Turner, D.P., Ritts, W.D., ... Saleska, S.R., 2006b. Evaluation of MODIS NPP and GPP products across multiple biomes. Remote Sens. Environ. 102, 282–292.

Van den Dool, Huug, Jin Huang, Fan, Yun, 2003. Performance and analysis of the constructed analogue method applied to US soil moisture over 1981–2001. J. Geophys. Res.-Atmos. 108, D16.

Van Oijen, M., Dreccer, M.F., Firsching, K.H., Schnieders, B.J., 2004. Simple equations for dynamic models of the effects of CO_2 and O_3 on light-use efficiency and growth of crops. Ecol. Model. 179, 39–60.

Veroustraete, F., Sabbe, H., Eerens, H., 2002. Estimation of carbon mass fluxes over Europe using the C-fix model and Euroflux data. Remote Sens. Environ. 83, 376–399.

Veroustraete, F., Sabbe, H., ... Bertels, L., 2004. Carbon mass fluxes of forests in Belgium determined with low resolution optical sensors. Int. J. Remote Sens. 25, 769–792.

Verstraeten, W.W., Veroustraete, F., Feyen, J., 2006. On temperature and water limitation of net ecosystem productivity: implementation in the C-fix model. Ecol. Model. 199, 4–22.

Wang, H., Prentice, I.C., Davis, T.W., 2014. Biophsyical constraints on gross primary production by the terrestrial biosphere. Biogeosciences 11, 5987–6001.
Wieder, W.R., Cleveland, C.C., ... Todd-Brown, K., 2015. Future productivity and carbon storage limited by terrestrial nutrient availability. Nat. Geosci. 8, 441.
Wu, D., Zhao, X., Liang, S., Zhou, T., Huang, K., Tang, B., Zhao, W., 2015. Time-lag effects of global vegetation responses to climate change. Glob. Chang. Biol. 21, 3520–3531.
Xiao, X., Zhang, Q., ... Ojima, D., 2004. Modeling gross primary production of temperate deciduous broadleaf forest using satellite images and climate data. Remote Sens. Environ. 91, 256–270.
Yan, H.M., Zhan, J.Y., ... He, W.J., 2016. Long time-series spatiotemporal variations of NPP and water use efficiency in the lower Heihe River Basin with serious water scarcity. Phys. Chem. Earth 96, 41–49.
Yang, S.H., Xu, J.Z., ... Wang, Y.J., 2016. Variations of carbon dioxide exchange in paddy field ecosystem under water-saving irrigation in Southeast China. Agric. Water Manag. 166, 42–52.
Yuan, W.P., Liu, S., ... Wofsy, S.C., 2007. Deriving a light use efficiency model from eddy covariance flux data for predicting daily gross primary production across biomes. Agric. For. Meteorol. 143, 189–207.
Yuan, W., Cai, W., ... Xia, J., 2014a. Vegetation-specific model parameters are not required for estimating gross primary production. Ecol. Model. 292, 1–10.
Yuan, W., Cai, W., ... Wohlfahrt, G., 2014b. Global comparison of light use efficiency models for simulating terrestrial vegetation gross primary production based on the LaThuile database. Agric. For. Meteorol. 192-193, 108–120.
Zhao, M.S., Running, S.W., 2010. Drought-induced reduction in global terrestrial net primary production from 2000 through 2009. Science 329, 940–943.